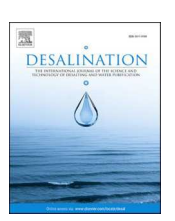
ELSEVIER

Contents lists available at ScienceDirect

Desalination

journal homepage: www.elsevier.com/locate/desal





Novel data-driven optimal control methods for cost-effective brine treatment

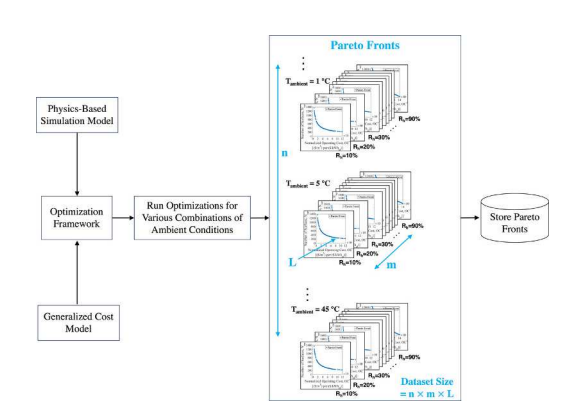
Mustafa F. Kaddoura*, Natasha C. Wright

Department of Mechanical Engineering, University of Minnesota, 111 Church Street SE, Minneapolis, MN 55455, USA

HIGHLIGHTS

- Data-driven optimal control methods are presented.
- Controller predicts optimal operation schedule based on weather forecast.
- Hybrid wind-fan operation reduces electric energy use.
- Operation in extreme cold weather
- Predictive, time-varying operation gave highest cost reduction.

GRAPHICAL ABSTRACT



ARTICLE INFO

Keywords: Cost Optimal Control Data driven Predictive Brine

$A\ B\ S\ T\ R\ A\ C\ T$

This study presents a novel data-driven optimal control method to minimize the cost of Convection-Enhanced Evaporation (CEE) systems under time-varying weather conditions. CEE is the approach of evaporating water from saline films (brine) on packed evaporation surfaces by air convection. Here, operating variables (brine injection rate, brine temperature, and air speed) are actively controlled as a function of current ambient conditions and daily weather forecast. The controller optimizes the process operation variables based on a dataset consisting of Pareto fronts, obtained in advance by solving a set of optimization problems. Three optimal operation strategies are presented: (1) real-time selection of operating variables, (2) predictive scheduled operation, and (3) hybrid wind-fan operation. The effectiveness of the proposed strategies was assessed through two case studies with distinct geographical locations and weather conditions: Alamogordo, New Mexico, and Minneapolis, Minnesota. The results show significant cost-saving potential relative to static operation. Predictive scheduled operation resulted in an annual average operating costs of \$0.91/m³ and \$6.63/m³ in Alamogordo and Minneapolis, respectively, with the higher costs in Minneapolis a result of the added thermal energy required to prevent freezing in winter.

E-mail address: kaddoura.mustafa@gmail.com (M.F. Kaddoura).

^{*} Corresponding author.

| Nomenclature | | Δp | pressure drop, Pa | |
|------------------|---|--------------------|---|--|
| | | r_I | material cost ratio, Wh _{el} /surface | |
| l | evaporation surface area, m ² | \boldsymbol{r}_2 | energy cost ratio | |
| р | specific heat, J/kgK | Rh | relative humidity, % | |
| CRF | capital recovery factor | T | temperature, K | |
| C | annualized capital cost, \$/year | ΔT | temperature difference, K | |
| C^* | normalized capital cost, (\$/year) per (\$/Whel) | Δt | operation time during of one year, hr | |
| sur | material cost of an evaporation surface, \$/surface | TC^* | normalized total cost, (\$/year) per (\$/Wh _{el}) | |
| fan | cost of a fan, \$/fan | и | air speed, m/s | |
| | vertical spacing between surfaces, m | \dot{V} | volumetric flow rate, m ³ /s | |
| vap | evaporation rate, kg/s | W | evaporation surface width, m | |
| | heat transfer coefficient, W/m ² K | Greek symbols | | |
| | specific enthalpy, J/kg | | • | |
| | interest rate, % | η_{fan} | fan efficiency, % | |
| | mass transfer coefficient, kg/m ² s | ω | moisture content, kg/kg | |
| el | cost of electric energy unit, \$/Wh _{el} | Subscri | ints | |
| m | material cost per evaporation surface, \$/surface | а | dry air | |
| th | cost of thermal energy unit, \$/Wh _{th} | e | exit conditions | |
| | evaporation surface length, m | el | electric | |
| i | mass flow rate, kg/s | g | gas phase (air-vapor mixture) | |
| | life time, years | in | inlet conditions | |
| I _{fan} | total number of fans | int | liquid-air interface | |
| I_{sur} | total number of evaporation surfaces | 1 | liquid phase | |
| I_{sI} | number of evaporation surfaces per evaporation module | sur | surface | |
| C | annual operating cost, \$/year | th | thermal | |
| C^* | normalized operating cost, (\$/year) per (\$/Whel) | ν | water vapor | |
| , | power consumption, W | | | |

1. Introduction

Desalination generates significant volumes of saline byproduct liquid known as brine, which is rich in desirable minerals [1]. Brine management is posing growing challenges from both environmental and economic perspectives, due to its potential environmental contamination and the substantial expenses linked to its treatment and/or disposal. Frequently researched methods for treating brine, such as brine crystallizers, can be expensive and require a significant amount of energy [2], particularly when used in smaller-scale applications (1-100 m³/day). To lower the expenses associated with brine treatment, two crucial approaches involve the creation of affordable, modular technologies and the systematic improvement of process operations [3]. By achieving cost-effective and modular solutions for brine treatment, it becomes possible to expand the application of inland desalination and enhance the safe management of brine in less regulated environments [4].

Few technologies are well-suited for addressing brine treatment in small-scale applications. Emerging membrane technologies include forward osmosis [5] and membrane distillation (MD). Evaporative technologies are another option for the treatment of extremely saline brine solutions, encompassing traditional evaporation ponds, wind-aided intensified evaporation (WAIV) [6], and humidification-dehumidification (HDH) [7].

In our prior research, we introduced convection-enhanced evaporation (CEE) as an innovative technique for concentrating brine through evaporation [8]. CEE involves a series of densely arranged hydrophilic evaporation surfaces, where liquid brine is distributed across the width of each surface, resulting in the formation of thin films. An air fan is employed to promote air movement over these films, establishing a vapor pressure differential between the air and the liquid, which drives the evaporation process. A mathematical model for CEE was developed and its performance was then assessed by comparing it to experimental findings for both horizontally packed [8] and vertically packed [9,10]

surfaces. Parametric analysis revealed that the key factors influencing both the performance and operational expenses are: (1) temperature of injected brine, (2) flow rate of brine, and (3) air flow speed [8,11]. Building on this understanding, an optimization framework which receives static ambient information and outputs the cost optimal operating variables was developed [12]. Nevertheless, it was observed that the system's performance deviates from its optimal state due to daily and seasonal fluctuations in weather conditions. Consequently, implementing real-time control of operational parameters based on weather conditions can lead to the reduction of operating costs, while still achieving a desired daily evaporation rate. Achieving this goal requires the development of an effective control strategy.

Desalination processes commonly employ Proportional-Integral-Derivative (PID) controllers due to their simplicity, reliability, and the existence of uncomplicated tuning guidelines [13]. Moreover, desalination processes have utilized non-linear model-based control and optimization-driven strategies to manage process parameters and attain specific production targets. McFall et al. [14] devised a model-based control system that combines nonlinear feedforward and feedback elements for high-recovery reverse osmosis desalination systems. This system was designed to counteract disruptions arising from variations in feedwater conditions, such as changes in flow rate or internal pressure. Self-optimizing control methods were also investigated for the control of desalination plant operation [15]. Another growing control method in the desalination and water treatment market is model-predictive controller (MPC) [16]. In one instance, Abbas [17] applied an MPC system for process control of reverse osmosis (RO) plant and observed significantly enhanced performance compared to traditional PI controllers. Similarly, Bartman et al. [18] introduced an MPC system tailored for an RO process with the aim of preventing water hammer incidents and mitigating pressure fluctuations. This approach could extend the predicted lifespan of equipment and contribute to optimizing system productivity. The mentioned control techniques can effectively sustain the process output at a designated level but do not prioritize the

optimization of energy usage or operational expenses, particularly in the presence of weather condition fluctuations [13].

Few scholars have focused on strategies that aim to reduce the energy usage within their control frameworks. Galizia [19] introduced a fuzzy control system designed for optimizing RO process, with the goal of minimizing the operation expenses in water reclamation facilities. Bartman et al. [20] considered minimizing the energy usage in RO plants by applying optimization-based control techniques. They also proposed scheduled operation as a potential avenue for future research to further enhance energy efficiency. Ghobeity and Mitsos [21] also applied optimization techniques to achieve an optimal, time-varying operation of RO plant with the aim of minimizing the daily electric energy usage. Their research demonstrated increased electricity savings by designing the plant with extra capacity (oversizing) and enabling shutdown during peak electricity cost periods. The drawback of these approaches is the necessity to real-time optimization which is in most cases not possible. This constraint restricts the applicability of optimization to problems that converge rapidly [20].

Recent studies has addressed some of the gaps commented above. Gil et al. [22] presented an Extremum-Seeking Control (ESC) approach to enhance the performance of solar membrane distillation for high salinity feeds. Two controllers were presented, in which the first one reduces thermal energy use by adapting the feed flow rate, and the second tries to find a trade-off between energy usage and water production. In addition, Gil et al. [23] also presented an online feedback optimization (OFO) to minimize thermal energy consumption while considering the variation in solar irradiation and brine salinity. The main idea behind the OFO is to consider the optimization algorithm as a dynamic system and include it in a feedback controller. Zhu et al. [24] proposed a model free bang-bang controller for membrane distillation to alleviate membrane scaling in solar membrane distillation. Eleiwi and Laleg-Kirati [25] presented a Lyapunov based controller to stabilize the temperature difference across the DCMD membrane has been proposed. Furthermore, Karam and Laleg-Kirati [26] have applied model predictive control to solar-thermal direct contact membrane distillation leading to a simplified model-free optimal controller for performance enhancement.

In this study, we devise a new data-driven optimal control method for reducing the operational expenses of CEE system, taking into consideration the fluctuation in weather conditions, while ensuring the desired daily evaporation rate as per the system's design specifications. To the best of authors' knowledge, this is the first study to present a real-time optimal control of CEE systems. This work:

- Introduces a novel data-driven control method to minimize the cost of CEE system in response to time-varying ambient conditions, while achieving a desired evaporation target;
- Introduces a scheduled operational approach based on weather forecast to predicts an optimal operational schedule, which includes shutting down the system during high operating cost periods and operating it either at full or partial capacity during other periods; and
- Investigates a hybrid operation that integrates naturally occuring wind availability with fan usage to decrease the electric energy usage, further reducing the operating cost.

Subsequently, we evaluate the effectiveness of three approaches in two case studies to demonstrate the cost savings achieved. The presented contributions enable CEE systems to continuously update its operation to maintain the most cost-efficient state over various weather conditions, resulting in a substantial reduction in the overall operational cost.

2. Proposed approach

The devised optimal control approach in this study aims to achieve two objectives: (1) attain the targeted daily evaporation rate amidst changing ambient conditions, and (2) minimize operational expenses (energy cost). This approach fundamentally converts a control problem into an optimization one, wherein the target evaporation rate (the controller's setpoint) is regarded as an optimization constraint, and the operational cost serves as the objective function to be minimized. Recognizing the significant computational demands of real-time optimization, an alternative data-driven approach is introduced.

2.1. Method 1: Time-varying optimal control approach informed by data analysis

Fig. 1 shows the proposed data-driven optimal operation control method based on time-varying ambient conditions. The method consists of two phases: (a) *data preparation*, which includes generating a dataset consisting of cost-optimal operating variables across distinct permutations of ambient temperature and ambient humidity, and (b) *control strategy*, which includes gathering real-time weather data at regular intervals and the system responding with the cost-optimal operational variables

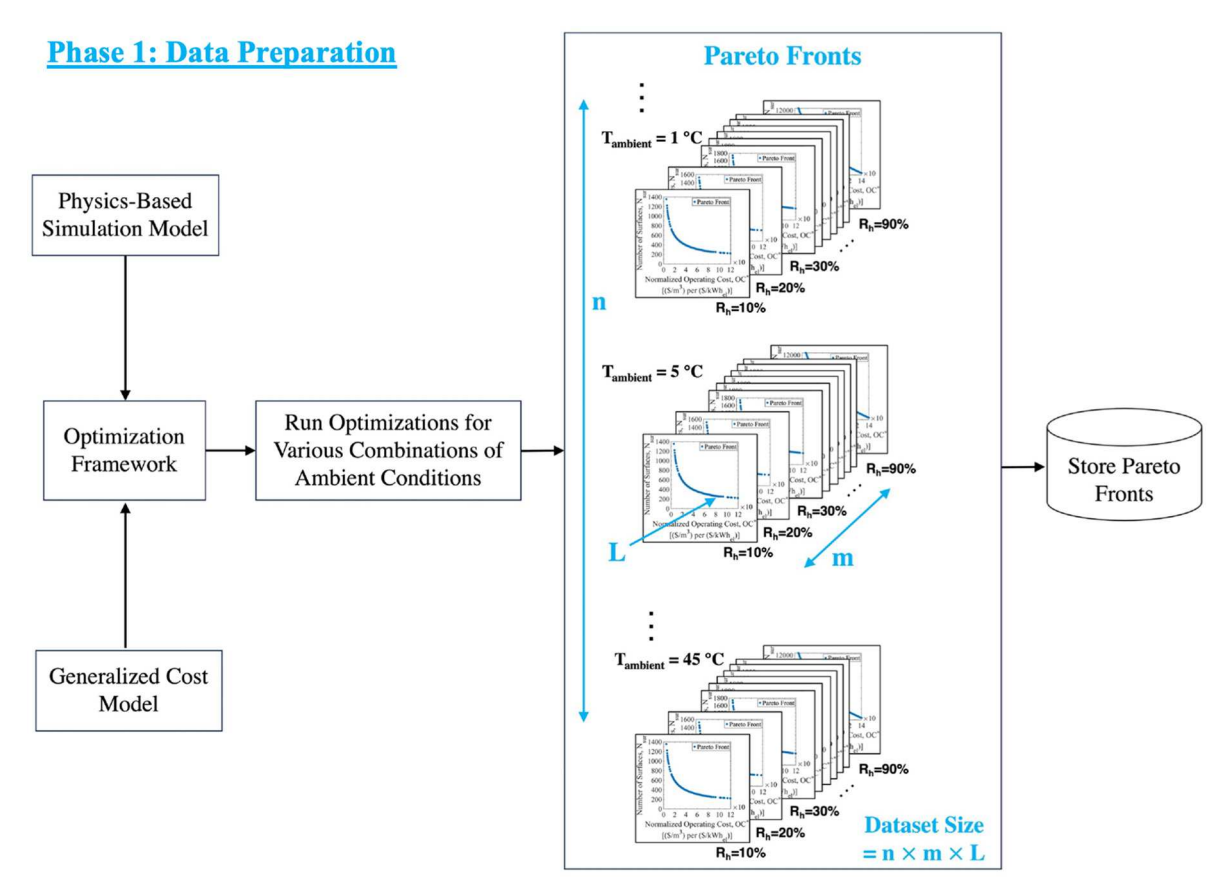
Physics-informed optimization-based data is generated in the data preparation phase as follows (Fig. 1a):

- 1. A physics-based system-level simulation model capable of predicting the performance of CEE system as a function of operating variables and prevailing weather conditions is implemented, as summarized and discussed in-depth in Kaddoura et al. [8].
- 2. A generalized cost model using cost ratios rather than absolute costs is used to predict the initial capital cost and the ongoing operational cost of each system design, as summarized and discussed in-depth in Kaddoura and Wright [12].
- 3. Using the models obtained in (1) and (2), a multi-objective optimization is conducted involving two objective functions, capital cost and operational cost, subject to prescribed design constraints (e.g. evaporation rate).
- 4. The optimization problem of (3) is executed for various permutations of weather conditions (temperature and humidity) and cost ratios, resulting in a set of Pareto fronts. Each Pareto front describes a family of cost-optimal operational variables for different system sizes (footprint areas).
- The acquired Pareto fronts, compromising of cost-optimal control variables consisting of flow rate and temperature of injected brine, and fan speed, are saved in a database contingent on varying system sizes.

After the dataset is created, it is stored in the memory of the controller. Figure1b illustrates the control approach applied in the second phase. At the start of every time interval, the controller receives the real-time sensor measurement of ambient temperature and humidity. Subsequently, the controller retrieves from the dataset the Pareto front that matches the closest environmental conditions. In this example, data was generated in steps of 5 °C and 10 % relative humidity. Each individual Pareto front illustrates the trade-offs between the operational expenses and the quantity of surfaces (system size), with N_{max} representing the maximum number of surfaces on the Pareto front. More operating surfaces leads to reduced operational expenses as less heating is required, and conversely, as was thoroughly discussed in our prior study [12]. Every point on the Pareto front represents a design vector encompassing optimal operating variables (brine flow rate and temperature, and fan speed) aligned with a particular system size and associated operating expenses. The controller tends to shift the design point along the Pareto front and select the system size that minimizes the cost constrained by the number of surfaces installed in the field, $N_{\text{Field}}. \\$ According to this description, three instances can exist (Fig. 1b):

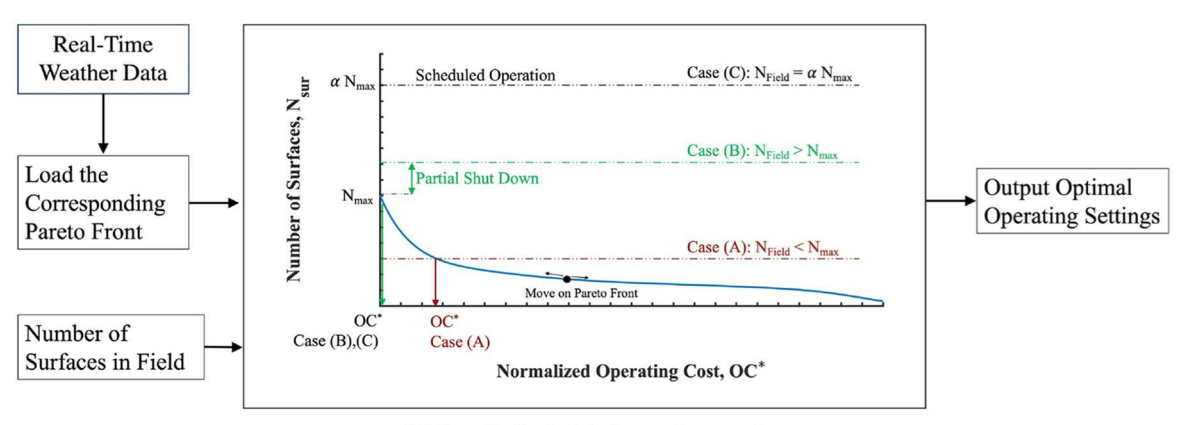
 $\bullet \ \ Instance \ (I): N_{Field} < N_{max}$

In this instance, the controller will tend to utilize all available sur-



(a) Phase 1: Data preparation and preprocessing.

Phase 2: Control Strategy



(b) Phase 2: Control strategy and approach.

Fig. 1. Diagram depicting the architecture of the proposed control method. In Phase 1, we create a dataset of cost-optimal operational variables for several permutations of ambient temperature and relative humidity. Subsequently, the resulting Pareto fronts are stored. In Phase 2, the controller receives real-time data weather data, which is then used to determine the optimal operational conditions in accordance to three cases (A, B, and C).

faces to minimize the operational cost. As a result, the controller will slide the design point towards the left side of the Pareto front until $N_{\text{sur}} \approx N_{\text{Field}}.$

 \bullet Instance (II) - Partial Shut Down: $N_{Field} > N_{max}$

In this instance, there are surplus field surfaces. The controller will aim to operate the system at $N_{\text{sur}}=N_{\text{max}}$ to minimize the operational cost, deactivating any excess surfaces (excess system modules) beyond

 N_{max} . We refer to this instance is as partial shut down.

• Instance (III) - Predictive Operation: $N_{Field} = \alpha N_{max}$

In this instance, the number of surfaces installed in the field is greater than N_{max} by a factor $\alpha.$ Considering a case where α is 2, the controller can activate all the available surfaces resulting in doubling the evaporation rate within that time interval. This strategy allows the controller to completely shut down the system during times of the day when un-

favorable environmental conditions would result in costly operation. This is referred to as *predictive operation*.

Fig. 2 elaborates data flow from the sensors, to controller, and finally to system actuators which include the pump, heat source, and modules' fans. CEE system installed in the field is composed of a series of evaporation modules, with each module containing a collection of parallelly arranged evaporation surfaces. Brine is fed to the CEE modules from a buffer tank which holds the brine generated from the desalination or industrial process. At the start of each time interval, the controller receives real-time sensor measurement of weather conditions, including temperature and humidity, as input variables, and provides the actuators with the cost-optimal values of operation variables (brine flow rate and temperature, and fan speed). This control method empowers the CEE to function autonomously, optimizing its operation according to prevailing weather conditions. In the following subsections, we will present the cost and performance models along with the optimization workflow used to generate the dataset of Pareto fronts.

2.1.1. Cost model

For the cost model (in Fig. 1a), we utilize the generalized cost model which we devised and thoroughly discussed in our previous work [12]. The initial capital cost includes the material cost of evaporation surfaces, fans, piping, buffer tank, labor cost, etc., which are all lumped into the material cost per evaporation surface coefficient, Ψ_m . The operational cost includes the cost of electric energy to drive the fans, and thermal energy required for preheating the brine to the desired temperature as specified by the controller. The model tends to normalize the capital cost and the operational cost by the cost of electric energy unit, Ψ_{el} , to generalize the Pareto fronts (optimization results) across different local cost scenarios (e.g. electric energy can be provided at different costs according to its source, such as from the grid, photovoltaics, diesel generators, etc. and thermal energy from solar thermal, waste heat recovery, burning of natural gas, etc.). The capital cost is given as

$$CC = \Psi_m \ N_{sur} \ CRF,$$
 (1)

and the normalized capital cost as

$$CC^* = \frac{CC}{\Psi_{el}} = r_1 \ N_{sur} \ \text{CRF}, \tag{2}$$

where N_{sur} is the number of evaporation surfaces installed in the field, CRF is the capital recovery factor, and r_1 is the material cost ratio given by

$$r_I = \frac{\Psi_m}{\Psi_{ol}}. (3)$$

The operating cost of CEE is expressed as

$$OC = (\Gamma_{el,sur} \ \Psi_{el} + \Gamma_{th,sur} \ \Psi_{th}) \ N_{sur} \ \Delta t, \tag{4}$$

and the normalized operating cost as

$$OC^* = (\Gamma_{el,sur} + \Gamma_{th,sur} \ r_2) \ N_{sur} \ \Delta t, \tag{5}$$

where $\Gamma_{el,sur}$ is the electric power consumption per surface, $\Gamma_{th,sur}$ is the thermal power consumption per surface, Ψ_{th} is the cost of thermal energy unit, Δt is the operation time duration, and r_2 is the energy cost ratio defined as

$$r_2 = \frac{\Psi_{th}}{\Psi_{ol}}. (6)$$

Formulating the capital cost (Eq. (2)) as a function of the material cost ratio, r_1 , irrespective of material cost of individual components generalizes the capital cost formulation to various market factors such as location, inflation, etc.. Similarly, formulating the operating cost (Eq. (5)) as a function of energy cost ratio, r_2 , irrespective of individual costs of electric and thermal energy generalizes the operating cost formulation to various sources and costs of energy. If the values of Ψ_m , Ψ_{th} , and Ψ_{el} are varied such that their ratios, r_1 and r_2 , are held constant, the normalized capital cost and the normalized operating cost are not affected. This allows the presented results of the current study to be generalizable to any combination of Ψ_m , Ψ_{th} , and Ψ_{el} [12]. Therefore, each value of material cost ratio, r_1 , and energy cost value, r_2 , simulate a distinct material and energy scenario in terms of price, source, and location. For the reader to get a sense of the costs obtained in this study, normalized costs can be multiplied by the cost of electric energy unit, Ψ_{el} , to obtain the absolute cost. In this study, an example value for Ψ_{el} of $0.1/kWh_{el}$ is used [27].

Finally, costs are function of the number of surfaces installed in the CEE system which is a function of weather conditions, estimated as

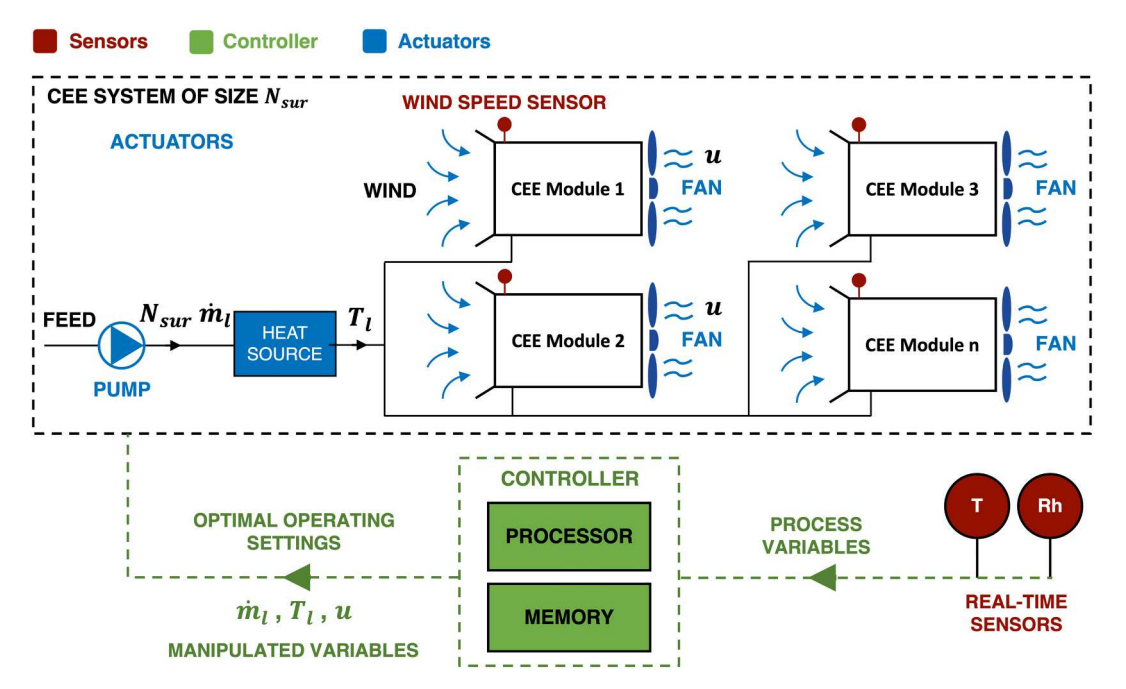


Fig. 2. Control diagram showing data flow between measurement sensors, controller, and CEE system.

$$N_{sur} = \frac{E_{vap,Target}}{E_{vap,sur}}. (7)$$

where $E_{vap,Target}$ and $E_{vap,sur}$ are target evaporation rate, and the nominal surface evaporation rate (m^3 /surface), respectively. The resulting cost model is dependent on weather conditions becasue $E_{vap,sur}$ is influenced by ambient temperature and humidity.

2.1.2. Performance model

The physics-based performance prediction model used to generate the data (in Fig. 1a) is based on conservation of mass and heat, solved numerically using the finite difference method. Mass and energy balances accompanied with interphase heat and mass transfer were derived by considering a control volume over an evaporation surface covered by a liquid (brine) film. Interfacial mass transfer (evaporation) is driven by the difference in moisture content between the air layer immediately adjacent to the liquid brine interface and the mean stream air. The rate of change of air enthalpy is due to the combination of the simultaneous sensible (convection) and latent (evaporation) heat transfer occurring at the air-liquid interface. A conservation of mass and conservation of energy within the control volume result in predicting the volume of liquid (brine) evaporated, the spatial temperature of liquid and air, and air humidity. The boundary conditions for the numerical model are the ambient conditions (air inlet temperature and humidity), liquid inlet conditions (flow rate and temperature), and air flow speed, which are used for solving the model equations. The pressure drop across the evaporation surfaces and the liquid inlet temperature are used to predict the electric and thermal energy used. Experimental validation via pilot testing showed good agreement between model predicted and experimentally measured evaporation rates with an error bounded between 10 % and 20 % for most cases [8]. The model outputs required for the cost model (Section 2.1.1) are the evaporation rate, $E_{vap,sur}$, and the electric and thermal energy use, $\Gamma_{el,sur}$ and $\Gamma_{th,sur}$, respectively.

2.1.3. Optimization framework and data preparation

In *Phase 1: data preparation*, a dataset of Pareto fronts is created offline by running a series of optimization problems at various permutation of ambient conditions. The optimization problem is set up as follows:

$$\min_{\mathbf{x}} \quad \mathbf{F}(\mathbf{x}, \mathbf{p})
\text{s.t. } \mathbf{G}(\mathbf{x}, \mathbf{p}) < 0,$$
(8)

F(x) is the objective function to be minimized, given as $F = [F_1, F_2]$, where F_1 is the normalized operating cost (Eq. (5)), and F_2 is the normalized capital cost (Eq. (2)). Note that F_2 is directly proportional to the number of evaporation surfaces, N_{sur} , therefore individual Pareto fronts resulting from this optimization cover optimal designs over a wide range of system sizes (footprint areas).

G(x) is the constraints function, given as $\mathbf{g} = [g_1, g_2] \leq 0$, (where)

$$g_1 = E_{vap,Target} - E_{vap,sur} N_{sur}. (9)$$

$$g_2 = 0^{\circ} C - T_{l,e}(^{\circ} C).$$
 (10)

where $T_{l,e}(^{\circ}C)$ is the temperature of the liquid exiting the evaporation surface. The first constraint (g_1) ensures achieving the target daily evaporation rate. The second constraint (g_2) prevents the brine from reaching the freezing point while flowing on the evaporation surface, in the case of cold weather.

Vector \mathbf{x} represents the design vector which includes (1) air flow speed, (2) flow rate of the brine per evaporation surface, and (3) inlet temperature of the brine, as optimization variables (manipulated control variables). The optimization was conducted for the following variable ranges: 1 L/h/surface to 6 L/h/surface for brine flow rate per surface, prevailing ambient temperature value to 90 °C for the inlet temperature of brine, and 1 m/s to 10 m/s for air flow speed. These operation

variables and their respective ranges were identified as having the most significant influence on energy usage and evaporation performance of CEE systems [8]. Finally, vector \mathbf{p} represents the constant model parameters vector which mainly includes the ambient temperature and relative humidity. The dataset is generated by creating permutations of the parameters vector \mathbf{p} .

The resultant Pareto front from solving the optimization problem illustrates the trade-offs between the operational expenses and the footprint area (represented by the number of surfaces or the capital cost), as shown in Fig. 1b. More operating surfaces leads to reduced operational expenses, and conversely. In this study, the dataset generated spans over diverse permutations of weather conditions which consist of fourteen values of ambient temperature (in the span of -20 °C to 45 °C with step increments of 5 °C) and ten values of ambient humidity (in the span of 10 % to 90 % with step increments of 10 % and an extra point at 85 %), which sums up to a 140 optimization cases and Pareto fronts. Each Pareto front contains 150 optimal designs, corresponding to various system sizes (N_{sur}); therefore, resulting in a total of 21,000 design points. Each design point represents an optimal design vector, x, consisting of the optimal operating variables. Due to cost formulation in terms of cost ratios, each Pareto front curve represents a family of cost scenarios as different combinations of costs can result in the same values of material and energy cost ratios, as discussed in Kaddoura et al. [12]. The material cost ratio and energy cost ratio considered in the dataset generated in this study are: r_1 55 kWh_{el}/surface and $r_2 = 0.25$; and it can be readily extended to include other ratios. The selected optimization algorithm is the nondominated sorting genetic algorithm II (NSGA-II) implemented in MATLAB (named as gamultiobj) [28,29]. Computations were conducted at Minnesota Supercomputing Institute (MSI). The average time for obtaining an optimization problem to converge ranges from 3 h to 6 h on 32 AMD CPU cores.

2.2. Method 2: Predictive operation approach

The ability of the controller to *predict* an optimal operation time plan using the weather forecast will further reduce the operational cost. This capability allows the system to completely shut down when the cost of energy usage is high, and to operate either at full capacity or with reduced capacity (partial operation) during other periods to further reduce operational costs, all while maintaining the desired evaporation rate.

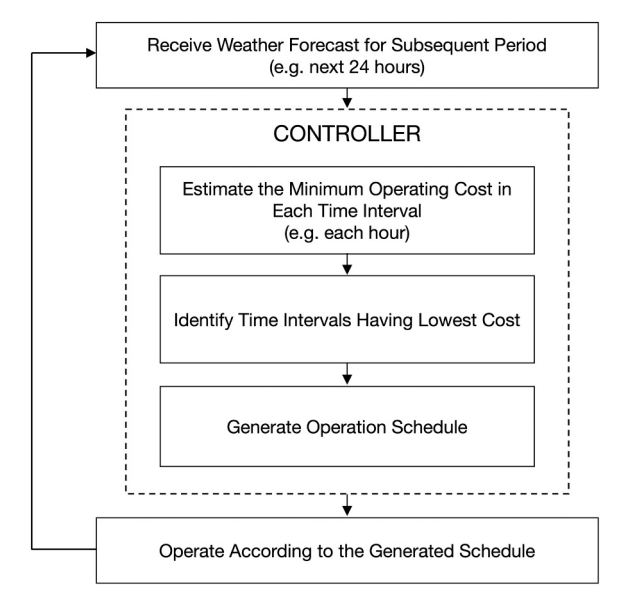


Fig. 3. Predicting optimal operation schedule.

The process of forecasting (predicting) an optimal operation schedule is illustrated in Fig. 3. First, the controller obtains weather forecast encompassing ambient temperature and relative humidity for a upcoming time frame, with this study focusing on a 24 h period. Second, the controller uses the weather forecast to simulate the system and predict the operational costs in the upcoming time frame (solely relying on the stored dataset of Pareto fronts as explained in Fig. 1b and Section 2.1). Third, the controller formulates an optimal operation timetable (schedule) by choosing the time intervals associated with the least expenses. In this study, the controller select 12 h duration from the initial 24 h time frame. Finally, the controller operates the system actuators according the generated schedule for the upcoming time frame. Its to be noted that the actual real-time control of the operating variables during the operation schedule is based on the real-time sensor measurement of prevailing ambient conditions, and is not relying on the forecast values. The forecast values are only used to predict the operational timetable (schedule).

2.3. Method 3: Combined wind-fan operation (hybrid approach)

To further reduce the electric power usage of the fan, we can utilize the natural airflow from the wind for evaporation. The control scheme of combining the wind-driven airflow and fan-driven airflow is illustrated in Fig. 4. The CEE modules are oriented parallel to the prevailing wind direction enabling wind to blow through them. In the cases where the wind matches the alignment of the CEE, the fan operates just to account for the disparity between the controller's preferred air speed (optimal value) and the wind speed currently accessible. This operation scenario allows CEE to utilize the evaporative potential of wind, whenever it is present, thereby enhancing the sustainability and energy efficiency of the CEE system.

3. Results and discussion

In this section, we present the outcomes obtained for a full year of hourly data simulation for two distinct geographical areas: Alamogordo, New Mexico, USA (32.8995° N, 105.9603° W) and Minneapolis, Minnesota, USA (44.9778 $^{\circ}$ N, 93.2650 $^{\circ}$ W). Alamogordo is the address of The Brackish Groundwater National Desalination Research Facility (BGNDRF), which is a focal point for developing technologies for the desalination of brackish and is a part of the Bureau of Reclamation, and its location offers a four-season climate enabling system evaluation under various weather conditions, while Minneapolis offers a very cold weather conditions. The objective is to evaluate the potential cost reductions achieved through the devised optimal control methods. Hourly temperature and relative humidity data for a representative year (2020) were acquired from NASA Prediction Of Worldwide Energy Resources (POWER) [30] (Figs. 5a, b and 10). An arbitrary optimal design was picked from the Pareto front to test the proposed control methods in this study.

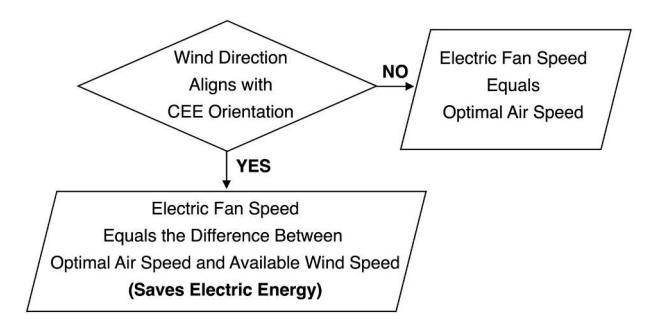
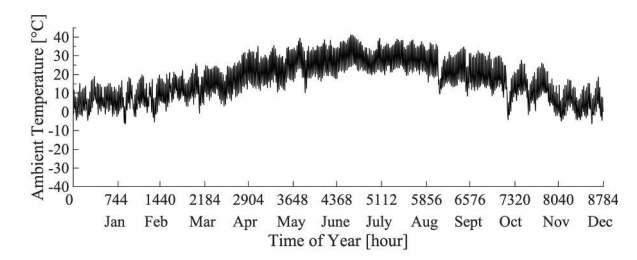
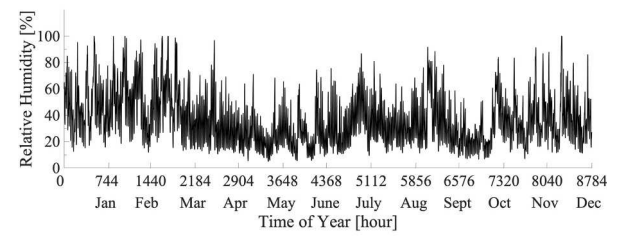


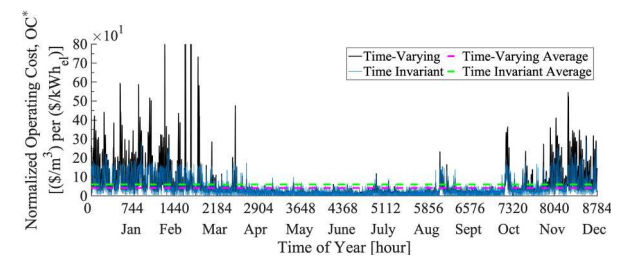
Fig. 4. Operation involving a combination of wind and fans.



(a) Alamogordo, New Mexico: Hourly profile of ambient temperature.



(b) Alamogordo, New Mexico: Hourly profile of ambient relative humidity.



(c) Operational cost comparison between time-varying strategy and time invariant strategy. The dotted lines represents the yearly mean cost.

Fig. 5. Profiles of ambient conditions [30] and resulting operating cost for Alamogordo, New Mexico.

3.1. Operational strategies and case studies

In this study, four operation strategies are explored, in which each strategy is a combination of the control methods discussed in Section 2:

- (A) Continuous, time invariant operation (baseline case): In this strategy, the operation of CEE system is optimized according to a single static value of ambient conditions (temperature and humidity) which represents the annual average values. Thus, the operating variables remain unchanged throughout the year, leading to hourly fluctuations in evaporation rate. This case is regarded as a baseline scenario for comparing the control methods outcomes against it.
- (B) Continuous, time-varying operation: This illustrates Method 1. In this scenario, the controller obtains the prevailing real-time ambient conditions at the beginning of each time interval, and accordingly modifies the operational variables to sustain the costoptimal operation. In this scenario, the system can enter a Partial Shut Down; however, it operates continuously (24/24 h).
- (C) Predictive scheduled operation: This illustrates the combination of Method 1 and Method 2. In this scenario, weather forecast are given to the controller to enable it to predict an optimal operation timetable (schedule) which minimizes the operational costs further, such as implementing a full shut down when the operational cost is high. This scenario results in a equal evaporation rate as in scenario (B).
- (D) Hybrid wind-fan operation: This illustrates the combination of *Method 1* and *Method 3*. In this scenario, the wind-driven air flow

is utilized along with the fan to induce evaporation. The system evaporates an equal volume as in scenarios (B) and (C).

Each of these four operation strategies are simulated for Alamogordo, New Mexico to access the cost savings in comparison to the baseline scenario (Strategy A). Next, these strategies were simulated for Minneapolis, Minnesota case to evaluate the controller's performance in severely cold weather conditions.

3.2. Continuous, time-varying strategy (Alamogordo)

The first strategy examined in this study is the continuous, time varying operation (strategy B) as opposed to the continuous, time invariant (static) operation (strategy A). In both scenarios, air flow is driven by electric fan, and the system operates continuously for 24 h per day. The purpose of this comparison is to evaluate the potential cost saving achieved when running the system with adaptable (optimized) operating settings based on prevailing ambient conditions. A comparison of the hourly normalized cost between strategy (B) (blue bars) and strategy (A) (black bars) are shown in Fig. 9. It is observed that the time-varying strategy leads to reduced hourly and annual operational costs since it consistently optimize its operating settings throughout the entire duration. The annual average cost savings accomplished by the controller is 28 % (from 6.0×10 (\$/m³) per (\$/kWh_{el})) to 4.32×10 (\$/m³) per (\$/kWh_{el})).

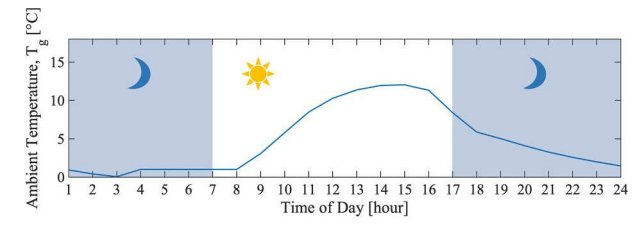
3.3. Predictive scheduled operation strategy (Alamogordo)

This section compares the predictive scheduled operation (strategy C) to the continuous, time invariant (static) operation (strategy A). Through this operation strategy, in addition to optimizing the operation in real-time, the system generates an optimal operation schedule based on weather forecast, and consequently the controller choose to operate the system during the 12 h corresponding to the lowest operational cost, as explained in Section 2.2. Fig. 6 shows an illustrative 24 h day example. Elevated humidity levels during night hours results in the highest operating costs (Fig. 6b). Therefore, the optimal operation schedule generated by the controller will include the 12 h corresponding the lowest predicted cost (between 9:00 and 20:00), and exclude the remaining 12 h (shut down the system). To achieve the daily evaporation target as in the continuous, time-varying case (strategy B), the installed number of evaporation surfaces implemented should be doubled, resulting in doubling the evaporation rate during the operation hours. Fig. 6d shows the normalized operating cost after applying the optimal operation schedule. The integration of the time-varying operation strategy in conjunction with the predictive operation led to a substantial decrease in the daily average operating cost (from 8.4×10 to $1.4 \times 10 \, (\$/m^3) \, \text{per} \, (\$/kWh_{el})$.

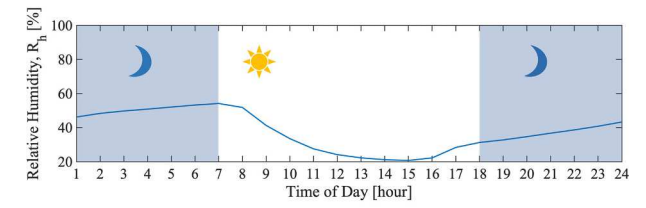
Finally, red bars in Fig. 9 show the normalized operational cost of strategy C which includes the integration of time-varying operation in conjunction with predictive scheduled operation. A substantial decrease in the annual normalized operating cost of 84 % is achieved (from 6.0×10 to 0.91×10 (\$/m³) per (\$/kWh_e_l)); this is equivalent to \$0.91/m³ at an example electricity unit cost of \$0.1/kWh_e_l which is considered economically competitive in comparison to other brine treatment technologies studied in the scientific literature.

To enable the scheduled 12-hour daily operation, it is necessary to oversize the system so that it can evaporate twice as much as water per hour compared the continuous 24-hour operation. However, the reduction in the operational cost may offset the additional capital cost required to oversize the system, as the operational cost dominates the capital cost, as we discussed in our prior research study on CEE system optimization [12], and as illustrated in the following paragraph.

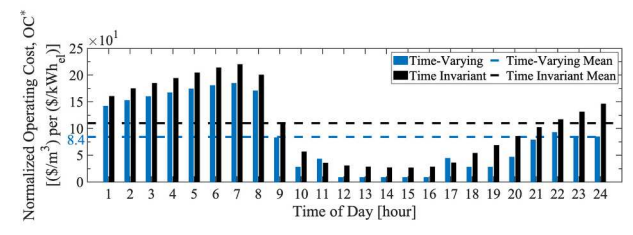
Fig. 7 demonstrates the increase in the capital cost against the reduction in the total cost resulted from oversizing the system in the predictive (scheduled) operation over various values of the material cost



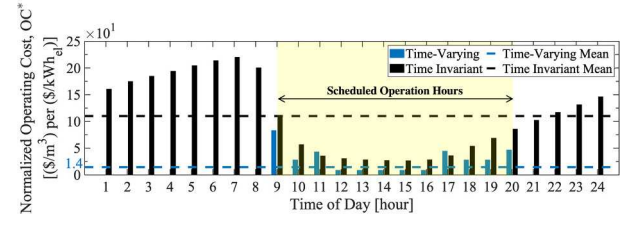
(a) Hourly profile of ambient temperature.



(b) Hourly profile of relative humidity.



(c) Operational cost comparison between *continuous* operation between time-varying scenario (strategy B) and time invariant scenario (strategy A).



(d) Operational cost comparison between *predictive, scheduled*, timevarying operation scenario (strategy C) and time invariant scenario (strategy A).

Fig. 6. An illustrative day example of scheduled, predictive operation scensrio (Alamogordo, New Mexico). Annual average costs is represented by dotted lines indicate.

ratio, r_1 (Eq.(3)). At a material cost ratio $r_1=27.5~{\rm kWh_{el}/surface}$, oversizing the system results in a 5.8 % increase in the capital cost; however, the total cost is reduced by 69.1 %. When the material cost is quadrupled to 110 kWh_{el}/surface, the increase in the capital cost becomes 19.8 %; however, the reduction in total cost is still dominating (44 %). At high material cost ratios (greater than 220 kWh_{el}/surface), the trend is changed in which the increase in the capital cost become larger than the savings in the total cost. As a conclusion, predictive scheduled operation with oversized system is economically beneficial for relatively low values of material cost ratios (less than 220 kWh_{el}/surface in this case).

3.4. Combined wind-fan hybrid operation strategy (Alamogordo)

This case study demonstrates strategy D which illustrates the advantage of the combined wind-fan operation (hybrid operation) in continuous, time-variant mode (discussed in Section 2.3). The controller optimizes the operating variables during each time interval over a 24 h operation per day.

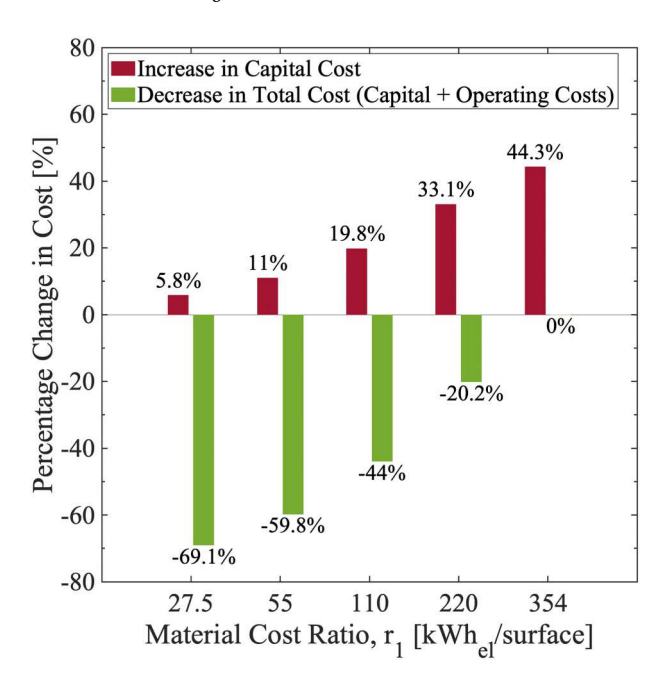


Fig. 7. Percentage change in system's capital cost and total cost (summation of capital cost and operational cost) resulting from oversizing the system in the predictive scheduled operation scenario. The potential operating cost savings surpass the increase in the capital cost.

The profile of wind speed and direction for Alamogordo, New Mexico is shown in Fig. 8. It is noticed that the prevailing wind direction predominantly falls within the southern sector within the angular range of 220 to 240. For that, the CEE system modules will be installed and aligned in the N-S direction to allow wind to naturally flows into the evaporation modules. During time intervals when the prevailing wind direction falls within the specified range [120° , 240°], the fan will operate a speed corresponding to the difference between the optimal airflow speed specified by the time-variant control strategy and the prevailing wind speed. Green bars in Fig. 9 shows the monthly normalized operating cost of the hybrid, time-varying case (strategy D). Utilizing the hybrid wind-fan operation resulted in 12% reduction in the electric energy usage and thus, the operational cost (from 4.32×10 to

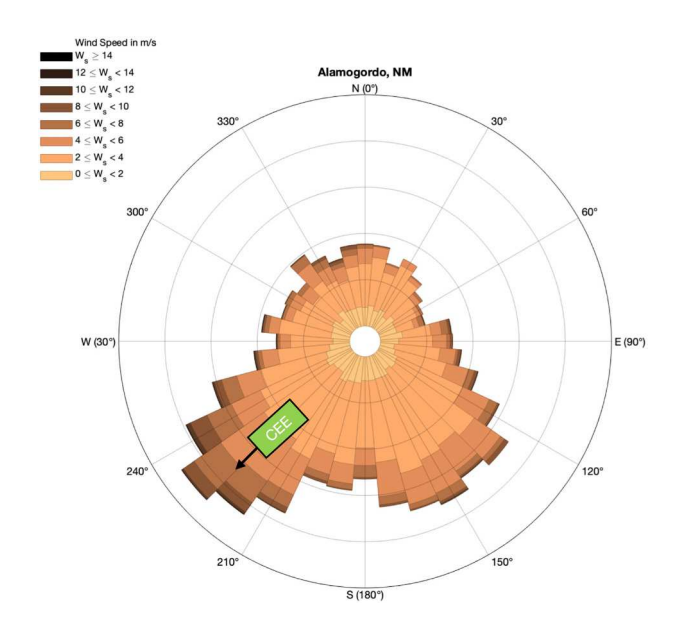


Fig. 8. Wind chart displaying the annual wind direction and speed data, and CEE alignment in the dominant wind direction (Alamogordo, New Mexico).

 $3.80 \times 10 \text{ ($/\text{m}^3$) per ($/\text{kWh}_{el}$))}.$

3.5. Summary of operational strategies results (Alamogordo)

Cost savings resulting from each operational strategy is illustrated in Table 1 and Fig. 9. As expected, the highest costs are obtained in the baseline case (continuous, time invariant operation) corresponding to a total cost of \$6.52/m³ and annual operating cost of \$6.0/m³, at an example electric energy unit cost, Ψ_{el} , of $\$0.1/kWh_{el}$. Strategy (B) (continuous, time-varying strategy) resulted in a cost reduction of 28 % (\$4.32/m3) at no additional capital cost. Strategy (D) (hybrid, timevarying, continuous operation) accomplishes an operational cost of 36 % (\$3.8/m³). It is noticed that the predictive operation (strategy C) has the most substantial effect on reducing the operating cost, bringing it down to \$0.91/m³, with an overall total cost reduction of 70 %; even though the capital cost is doubled. This agrees with the observations of Ghobeity and Mitsos [21] regarding RO system operation, in which they found that the major savings in electric energy usage was accomplished when oversizing the system enabling it to turn off during time periods of high energy cost. This also aligns with the future work recommended by Bartman et al. [20], who also advocated for scheduled operation of RO systems as a mean to decrease energy usage. Finally, the combination of the three strategies (predictive, hybrid, time-varying operation) leads a total cost savings of 74 % at an operating cost of $0.66/m^3$.

3.6. Severe cold weather scenario (Minneapolis)

The devised control methods in this study enable the system to operate in various weather conditions, in addition to reducing its operational costs. Minneapolis, Minnesota, USA is selected to evaluate the control methods in cold weathers (subzero temperatures) (Fig. 10). To overcome the risk of liquid freezing on the evaporation surfaces as the ambient temperature drops below 0 $^{\circ}$ C, the liquid must be preheated to a sufficient inlet temperature to avoid it reaching the freezing point while it undergoes evaporation. This condition is accommodated to via the optimization constraint presented in Eq. (10).

Fig. 11 presents an illustrative simulation depicting how the liquid (brine) outlet temperature (at the end of the evaporation surface) varies with changing ambient temperatures, considering various liquid preheat temperature (brine inlet temperature). For instance, when the ambient temperature is $-10\,^{\circ}\text{C}$, the liquid should be preheated to at least 30 $^{\circ}\text{C}$ to ensure its temperature does not drop below freezing point; also, when the ambient temperature is $-15\,^{\circ}\text{C}$, the liquid should be preheated to at least 50 $^{\circ}\text{C}$. As a result, colder climates require greater thermal energy usage to enable safe operation without freezing, leading to an increased operational cost.

Fig. 12 provides a summary of the monthly normalized operational costs over the course of the simulated year in Minneapolis, Minnesota. It is noticed that the time-varying operational strategy has a limited effect on reducing the operational costs, mainly due to the consistently high humidity throughout most days of the year. Nonetheless, applying the time-varying operation strategy becomes imperative in cold climates, as the inherent optimization constraint (Eq.(10)) ensures that the liquid does not freeze, thus facilitating safe system operation in cold conditions. Time invariant operation, on the other hand, carries the risk of freezing. Conversely, the predictive scheduled operational strategy has lowered the operational cost by approximately 53 % (from 14.3×10 $(\$/m^3)$ per $(\$/kWh_{el})$ to $6.63 \times 10 (\$/m^3)$ per $(\$/kWh_{el})$). The yearly average operational cost in Minneapolis case is about seven times higher than that in Alamogordo case, which is expected and attributed to the additional thermal energy usage needed to prevent liquid freezing, and also to the relatively higher levels of humidity in Minneapolis compared to Alamogordo.

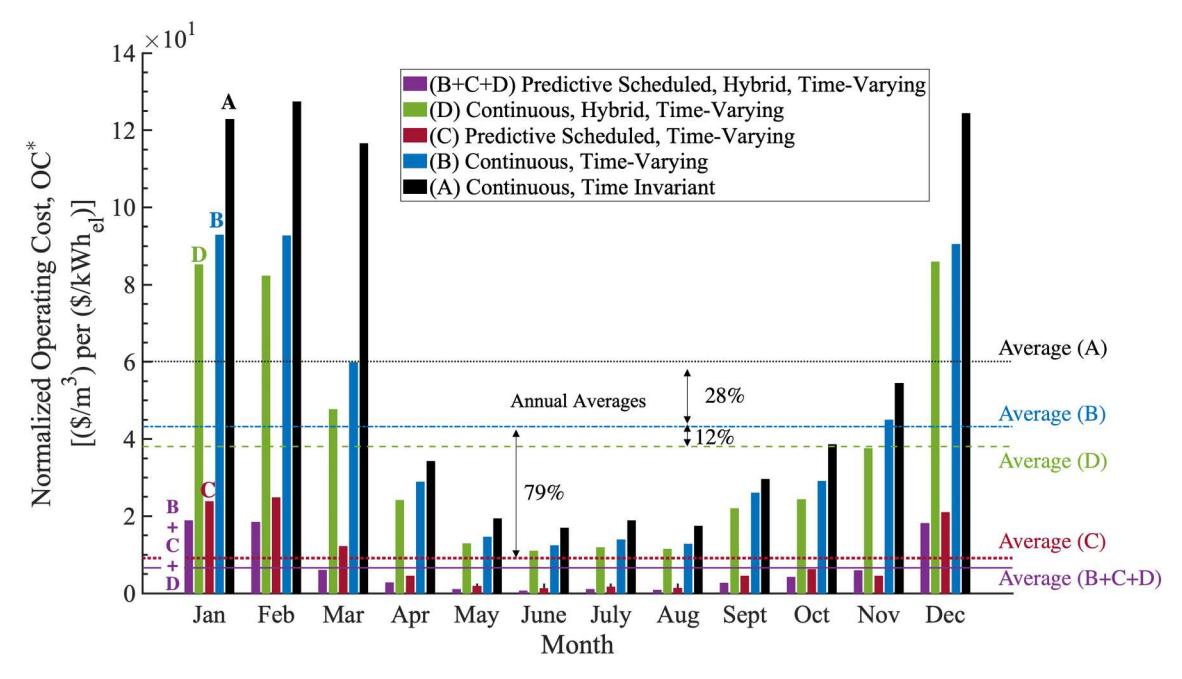
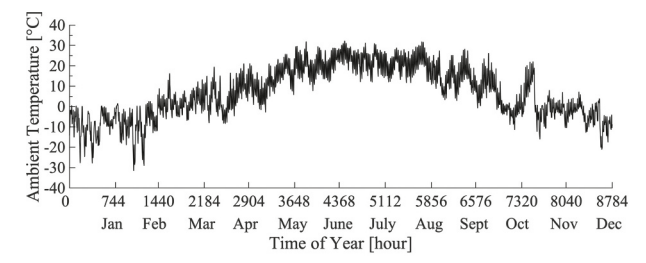


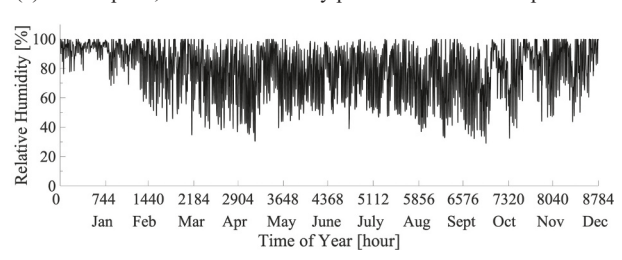
Fig. 9. Operating cost comparison across different operational strategies in Alamogordo, New Mexico. Annual mean costs are represented by dotted lines. Material and energy cost ratios of $r_1 = 55\,$ kWh_{el}/surface and $r_2 = 0.25$, respectively, are used in this study.

Table 1 Operational cost associated across each strategy in Alamogordo, New Mexico. An example cost of electric energy unit, Ψ_{el} , of $\$0.1/kWh_{el}$ is used in this table to convert normalized costs to absolute costs.

| Control Strategy | Continuous, time invariant - baseline | Continuous, time- varying | Continuous, hybrid, time- varying | Predictive scheduled, time- varying | Predictive scheduled, hybrid, time-varying |
|---------------------------------|---------------------------------------|------------------------------|--------------------------------------|--|--|
| | (strategy A) | (strategy B) | (strategy D) | (strategy C) | (strategies B + C + D) |
| Mean operating cost (\$/m³) | 6.0 | 4.32 | 3.80 | 0.91 | 0.66 |
| Capital cost (\$/m3) | 0.52 | 0.52 | 0.52 | 1.04 | 1.04 |
| Total cost (\$/m ³) | 6.52 | 4.84 | 4.32 | 1.95 | 1.70 |



(a) Minneapolis, Minnesota: Hourly profile of ambient temperature.



(b) Minneapolis, Minnesota: Hourly profile of ambient relative humidity.

Fig. 10. Profiles of ambient condition for Minneapolis, Minnesota [30].

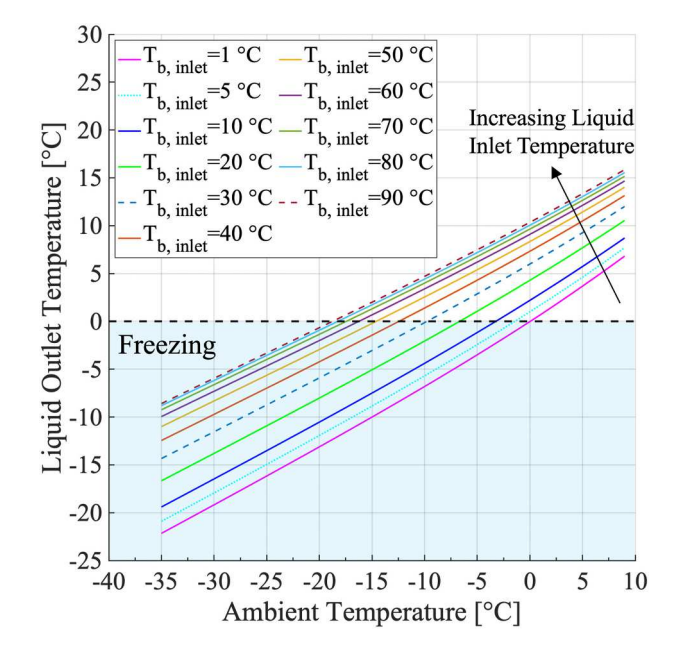


Fig. 11. Illustrative simulation showing liquid outlet temperature in relation to ambient temperature, under $60\ \%$ relative humidity.

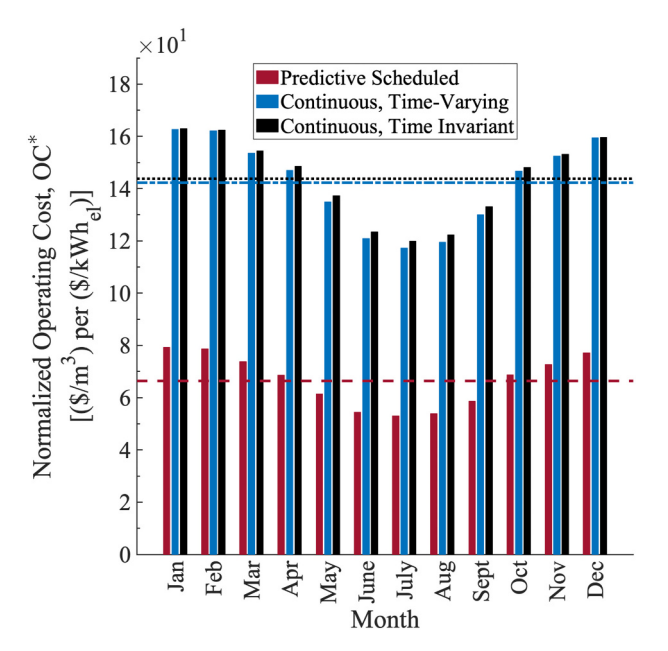


Fig. 12. Comparison of operational costs between the predictive (scheduled), continuous time-varying strategy and the continuous time invariant operation strategy in Minneapolis, Minnesota. Annual cost mean values are represented by dotted lines.

3.7. Uncertainty and real-world implementation

Although the proposed data-driven methods in this study show a high advantage in enabling CEE systems to maintain the most cost-efficient state over various weather conditions, uncertainties may arise in real-world implementation from the following sources:

- 1. Accuracy and uncertainty associated with the computed Pareto fronts (the generated dataset): The performance model used in Section 2.1.2 for dataset generation was experimentally validated via a pilot plant testing, and results showed good agreement between the model predictions and experimentally measured values, with an error bounded within 10 % and 20 % for most cases [8]. Errors or uncertainties associated with the computed Pareto fronts may result in either under-evaporating (evaporating lower volume than desired) or over-evaporating (evaporating larger volume than desired). This can be addressed in future work by adding feedback in the control loop (e.g. checking whether the targeted evaporation rate was achieved during each time interval, and compensating for any discrepancies in the next time interval).
- 2. Uncertainty in weather forecast: weather forecast of ambient temperature and humidity is only used to predict an optimal operation schedule (timetable); however, real-time control of the operating settings (liquid flow rate, temperature, and fan speed) is based on real-time sensor measurement. Thus, uncertainty in weather forecast will not have any effect on achieving the targeted evaporation setpoint, and is expected to only affect the predicted operation schedule, which will have a minimal impact on the overall process operation optimality.

Future work will include pilot testing of the developed control approach to assess the control methods/strategies experimentally under real-world conditions. Pilot testing will quantify the effects of the mentioned uncertainties, and lessons learned will act as a guideline for future enhancement of the controller.

4. Conclusion

This research introduces an innovative data-driven control approach to minimize the operational costs of CEE systems in real-time while adapting to time-varying weather conditions. The controller relies on a dataset comprising Pareto fronts derived from solving a series of optimization problems. Furthermore, the controller obtains weather forecasts to anticipate an optimal operation schedule, enabling predictive operation. Three approaches to reduce the cost were investigated: (1) adjusting operating variables over time, (2) implementing predictive scheduled operation, and (3) utilizing a hybrid wind-fan operation. The controller performance was assessed through two separate case studies set in two distinct geographical locations and weather conditions. The cost model used in this study relies on normalizing the capital and operating costs to generalize the controller results to various cost scenarios. Key findings include:

- In the continuous, time-varying operational strategy, the controller receives real-time measurement of prevailing ambient temperature and humidity during each time interval, and adjust the CEE system operational variables to minimize the operational cost. This strategy leads to 26 % reduction in the total cost in comparison to continuous, time invariant (static) operation.
- In the predictive scheduled operational strategy, the controller obtains weather forecast for the upcoming hours and accordingly generates an optimal operational schedule (timetable) to further minimize the cost. During the time periods corresponding to high operational costs (for example, humid hours), the controller turns off the system, and compensate for the decrease in evaporation rate at other times as the system is enlarged in this strategy. This leads to a total cost savings of 70 % in comparison to continuous, time invariant (static) operation. This strategy results in an operational cost of \$0.91/m³ and total cost of \$1.95/m³.
- In the combined wind-fan operation (hybrid approach), air flow is induced by a combination of natural wind and fan on the purpose of reducing the electric energy use of the fan. Applying this strategy led to cost savings of 34 % in comparison to the baseline case (continuous, time invariant (static) operation).
- When the three strategies (predictive scheduled, hybrid, timevarying operation) are integrated, it leads to a substantial 74 % cost savings. A total cost of \$1.70/m³ and an operating cost of \$0.66/m³ are achieved.
- The predictive scheduled operational strategy led to the most significant cost reduction (at low material cost ratios).
- In severe cold weather, it is imperative to preheat the liquid to avoid freezing and to enable CEE safe operation. Consequently, this lead to an increase in the operating cost. The predictive scheduled operation is still an effective strategy to minimize the cost.

The cost reductions attained through the proposed control strategies highlight CEE's potentials to serve as a cost-efficient solution for brine treatment. The case studies also illustrate how CEE can effectively adapt to various fluctuations in ambient conditions.

CRediT authorship contribution statement

Mustafa F. Kaddoura: Conceptualization, Methodology, Software, Visualization, Validation, Investigation, Formal analysis, Data curation, Writing - original draft, Writing - review & editing. **Natasha C. Wright:** Conceptualization, Methodology, Writing – review & editing, Supervision.

Declaration of competing interest

The authors declare that they have no known competing financial interests or personal relationships that could have appeared to influence the work reported in this paper.

Data availability

Data will be made available on request.

Acknowledgment

Funding for this project was provided by the US Bureau of Reclamation under Grant Number R21AC10130 and the Minnesota Environment and Natural Resources Trust Fund as recommended by the Legislative-Citizen Commission on Minnesota Resources (LCCMR). Computational resources were provided by the Minnesota Supercomputing Institute (MSI) at University of Minnesota.

References

- [1] A. Panagopoulos, K.J. Haralambous, Minimal Liquid Discharge (MLD) and Zero Liquid Discharge (ZLD) strategies for wastewater management and resource recovery-analysis, challenges and prospects, J. Environ. Chem. Eng. 8 (5) (2020) 104418, https://doi.org/10.1016/j.jece.2020.104418.
- [2] A. Panagopoulos, K.J. Haralambous, Environmental impacts of desalination and brine treatment - challenges and mitigation measures, Mar. Pollut. Bull. 161 (PB) (2020) 111773, https://doi.org/10.1016/j.marpolbul.2020.111773.
- [3] A.V. Dudchenko, T.V. Bartholomew, M.S. Mauter, High-impact innovations for high-salinity membrane desalination, Proc. Natl. Acad. Sci. U. S. A. 118 (37) (2021), https://doi.org/10.1073/pnas.2022196118.
- [4] S. Amrose, K. Cherukumilli, N.C. Wright, Chemical contamination of drinking water in resource-constrained settings: global prevalence and piloted mitigation strategies, Annu. Rev. Environ. Res. 45 (2020) 195–226, https://doi.org/10.1146/ annurey-environ-012220-105152.
- [5] M. Ahmed, R. Kumar, B. Garudachari, J.P. Thomas, Performance evaluation of a thermoresponsive polyelectrolyte draw solution in a pilot scale forward osmosis seawater desalination system, Desalination 452 (August 2018) (2019) 132–140, https://doi.org/10.1016/j.desal.2018.11.013.
- [6] J. Gilron, Y. Folkman, R. Savliev, M. Waisman, O. Kedem, WAIV wind aided intensified evaporation for reduction of desalination brine volume, Desalination 158 (1–3) (2003) 205–214, https://doi.org/10.1016/S0011-9164(03)00453-3.
- [7] G.P. Narayan, M.H. Sharqawy, V. J. H. Lienhard, S.M. Zubair, Thermodynamic analysis of humidification dehumidification desalination cycles, Desalin. Water Treat. 16 (1–3) (2010) 339–353, https://doi.org/10.5004/dwt.2010.1078.
- [8] M.F. Kaddoura, M. Chosa, P. Bhalekar, N.C. Wright, Mathematical modeling of a modular convection-enhanced evaporation system, Desalination 510 (2021) 115057, https://doi.org/10.1016/j.desal.2021.115057.
- [9] M.F. Kaddoura, N.C. Wright, Design comparative analysis of convection-enhanced evaporation systems, Appl. Therm. Eng. 225 (February) (2023) 120188, https:// doi.org/10.1016/j.applthermaleng.2023.120188.
- [10] M.F. Kaddoura, N.C. Wright, Assessment of convection-enhanced evaporation (CEE) design: a comparison of flow configurations, SSRN Electron. J. (2022), https://doi.org/10.2139/ssrn.4189446. URL, https://www.ssrn.com/abstract -4189446
- [11] N. Guillen Rodriguez, M.F. Kaddoura, N.C. Wright, Modeling a Concentrated Solar Collector (CSC) - Convection-Enhanced Evaporation (CEE) System for Small-Scale Brine Management, in: Volume 3A: 49th Design Automation Conference (DAC), American Society of Mechanical Engineers, 2023, https://doi.org/10.1115/ DETC2023-117236.

- [12] M.F. Kaddoura, N.C. Wright, Optimization of convection-enhanced evaporation (CEE) using generalized cost ratios, Water Res. 219 (April) (2022) 118491, https://doi.org/10.1016/j.watres.2022.118491.
- [13] G.P. Rao, D.M.K. Al-Gobaisi, A. Hassan, A. Kurdali, R. Borsani, M. Aziz, Towards improved automation for desalination processes, part II: intelligent control, Desalination 97 (1–3) (1994) 507–528.
- [14] C.W. McFall, A. Bartman, P.D. Christofides, Y. Cohen, Control of a reverse osmosis desalination process at high recovery, Proc. Am. Contr. Conf. (2008) 2241–2247, https://doi.org/10.1109/ACC.2008.4586825.
- [15] S. Skogestad, Plantwide control: the search for the self-optimizing control structure, J. Process Control 10 (5) (2000) 487–507, https://doi.org/10.1016/ S0959-1524(00)00023-8.
- [16] M.F. Kaddoura, Simulation and optimization of energy systems, in: E. Zio, P. M. Pardalos, M. Fathi (Eds.), Handbook of Smart Energy Systems, Springer International Publishing, Cham, 2022, pp. 1–77, https://doi.org/10.1007/978-3-030-72322-4 146-1.
- [17] A. Abbas, Model predictive control of a reverse osmosis desalination unit, Desalination 194 (1–3) (2006) 268–280, https://doi.org/10.1016/j. desal 2005 10 033
- [18] A.R. Bartman, C.W. McFall, P.D. Christofides, Y. Cohen, Model-predictive control of feed flow reversal in a reverse osmosis desalination process, J. Process Control 19 (3) (2009) 433–442, https://doi.org/10.1016/j.jprocont.2008.06.016. URL, https://doi.org/10.1016/j.jprocont.2008.06.016.
- [19] A. Galizia, J. Mamo, G. Blandin, M. Verdaguer, J. Comas, I. Rodríguez-Roda, H. Monclús, Advanced control system for reverse osmosis optimization in water reuse systems, Desalination 518 (2021), https://doi.org/10.1016/j. desal.2021.115284.
- [20] A.R. Bartman, A. Zhu, P.D. Christofides, Y. Cohen, Minimizing energy consumption in reverse osmosis membrane desalination using optimization-based control, J. Process Control 20 (10) (2010) 1261–1269, https://doi.org/10.1016/j. jprocont.2010.09.004.
- [21] A. Ghobeity, A. Mitsos, Optimal time-dependent operation of seawater reverse osmosis, Desalination 263 (1–3) (2010) 76–88, https://doi.org/10.1016/j. desal.2010.06.041.
- [22] J.D. Gil, L. Roca, G. Zaragoza, M. Pérez, M. Berenguel, Improving the performance of solar membrane distillation processes for treating high salinity feeds: a process control approach for cleaner production, J. Clean. Prod. 338 (2022) (April 2021), https://doi.org/10.1016/j.iclepro.2022.130446.
- [23] J.D. Gil, A. Bueso, L. Roca, G. Zaragoza, M. Berenguel, Data-driven online feedback optimization of solar membrane distillation systems operating in batch mode, J. Process Control 129 (2023) 103056, https://doi.org/10.1016/j. iprocont.2023.103056.
- [24] Z. Zhu, W. Wang, Q. Zhang, X. Chen, Insight into the feed/permeate flow velocity on the trade-off of water flux and scaling resistance of superhydrophobic and welding-pore fibrous membrane in membrane distillation, J. Membr. Sci. 620 (2021) 118883, https://doi.org/10.1016/j.memsci.2020.118883. URL, https://li nkinghub.elsevier.com/retrieve/pii/S0376738820314587.
- [25] F. Eleiwi, T.M. Laleg-Kirati, Observer-based perturbation extremum seeking control with input constraints for direct-contact membrane distillation process, Int. J. Control. 91 (6) (2018) 1363–1375, https://doi.org/10.1080/ 00207179.2017.1314551.
- [26] P. Bendevis, A. Karam, T.M. Laleg-Kirati, Optimal model-free control of solar thermal membrane distillation system, Comput. Chem. Eng. 133 (2020) 106622, https://doi.org/10.1016/j.compchemeng.2019.106622.
- [27] U.E.I. Administration, U.S. Energy Information Administration (EIA), URL, https://www.eia.gov/.
- [28] MATLAB, MATLAB, 2020.
- [29] K. Deb, Multi-objective Optimization Using Evolutionary Algorithms Kalyanmoy Vol. 16, 2001 (arXiv:arXiv:1011.1669v3).
- [30] NASA, Prediction of Worldwide Energy Resources, URL, https://power.larc.nasa.gov/.